Astron. Astrophys. 363, 141–153 (2000)

ASTRONOMY AND ASTROPHYSICS

Radio-loud active galaxies in the northern ROSAT All-Sky Survey

IV. Properties of sources stronger than 100 mJy at 5 GHz⋆

W. Reich[1], **E. Fürst**[1], **P. Reich**[1], **R. Kothes**[1,⋆⋆], **W. Brinkmann**[2], **and J. Siebert**[2]

[1] Max-Planck-Institut für Radioastronomie, Auf dem Hügel 69, 53121 Bonn, Germany
[2] Max-Planck-Institut für Extraterrestrische Physik, Giessenbachstrasse, 85740 Garching, Germany

Received 8 February 2000 / Accepted 8 August 2000

Abstract. We present multi-frequency radio data for 741 extragalactic sources with a 5 GHz integrated flux density of > 100 mJy. These sources have been selected from a cross-correlation of an early ROSAT All-Sky Survey source list with a list of compact radio sources of the 5 GHz Green Bank northern sky survey (RGB sample). The majority of sources were quasi-simultaneously observed with the Effelsberg 100-m telescope at 11 cm, 6 cm, and 2.8 cm. We have determined the spectrum, size and linear polarization properties of these sources. We compare the radio data with ROSAT measurements and optical data. We find that the X–ray selected radio sources, when compared with unbiased radio source samples, are on average slightly more compact, show a higher fractional polarization, a higher absolute rotation measure (RM), and have flatter spectra. Absolute RMs are larger for steep spectrum than for flat spectrum sources and for extended than for compact sources. The average redshift increases with the radio flux density, which indicates that the X–ray selected radio sources have a larger fraction of beamed radio emission. All source characteristics of the sample are in accordance with present unification schemes for AGN, where X–ray selected sources are preferable looked at face on.

Key words: polarization – galaxies: active – quasars: general – radio continuum: general – X-rays: general

1. Introduction

Radio-loud active galactic nuclei (AGN) present a small but distinctive subgroup of extragalactic objects. To understand their general properties and to be able to distinguish the various subclasses of this population a large number of sources needs to be studied in order to minimise the inherent selection effects and to be able to draw statistically firm conclusions about the roles of the various observable source parameters. The required large number of sources is most conveniently found from large unbiased sky surveys in different frequency bands.

While several large area radio surveys with high sensitivity are available the X–ray data for AGN usually originate from pointed observations or from limited X–ray surveys with low sensitivity. The ROSAT All-Sky Survey (RASS) was the first soft X–ray survey of the whole sky using an imaging telescope (Trümper 1983) with a limiting sensitivity of a few 10^{-13} erg cm^{-2} s^{-1}. The cross-correlation of the RASS source list (Voges 1992) with existing radio source catalogues yielded a comprehensive sample of radio-loud extragalactic X–ray sources with unprecedented low sensitivity limits of the radio and X–ray catalogues.

In previous papers (Brinkmann et al. 1995 (B95), Brinkmann et al. 1997b (B97)) we presented the results of a cross–correlation of the ROSAT All-Sky Survey source list with a radio source list generated from the Condon et al. (1989) 5 GHz survey of the northern sky (RGB = RASS - Green Bank sources). With 2127 coincidences, the RGB is one of the largest well–defined flux density limited surveys of AGN ever obtained. Note that the RGB pushes 1–2 orders of magnitude deeper in both X–ray and radio flux density compared to previous unbiased wide-area AGN surveys.

Only 617 of the sources had been previously optically identified as extragalactic objects (B95), usually those with higher radio and X–ray flux densities.

All sources have been studied at the VLA in snapshot mode (Laurent-Muehleisen et al. 1997, L97) to obtain arcsec positions and 5 GHz core flux densities. With these accurate positions it was possible to find plausible optical counterparts for most of the sources from digitized POSS plates (McMahon 1991). A discussion of the broad band, radio to X–ray, bulk properties of the unidentified objects has been given recently in B97. It turned out that any analysis based on objects with existing classifications only is bound to be biased towards sources with extreme properties in at least one of the observing bands, mostly high flux densities. The majority of the new RGB sources have broad-band properties between those of traditional radio-selected and

Send offprint requests to: W. Reich (wreich@mpifr-bonn.mpg.de)

⋆ Tables 1 and 2 are only available in electronic form at the CDS via anonymous ftp to cdsarc.u-strasbg.fr (130.79.128.5) or via http://cdsweb.u-strasbg.fr/Abstract.html

⋆⋆ *Present address:* Dominion Radio Astrophysical Observatory, National Research Council of Canada, P.O. Box 248, Penticton, BC V2A 6K3, Canada

X–ray selected AGN. There is no bimodal distribution in the radio-loudness distribution, and the traditional division between radio-loud and radio-quiet AGN might not be warranted.

Strong correlations between radio and X–ray properties were found for the different classes of objects (e.g. B95, B97). However, the radio properties had to be taken from previously published data which were obtained non-simultaneously in the different frequency bands. Keeping in mind that radio-loud AGN show, in general, substantial temporary variability, any correlation involving radio properties like radio-loudness, core dominance, or spectral slope must contain a certain degree of systematic scatter. Therefore, a program was initiated to measure the multi-frequency radio properties of a large number of AGN quasi-simultaneously.

The outline of the paper is as follows. In the next section we will give an overview on the contents and the properties of the used source catalogues, the selection criteria and further information on the source properties. In Sect. 3 we will describe the radio observations with the Effelsberg 100-m telescope and present the results in the form of a source catalogue including the ROSAT X–ray flux density and other relevant information. The X–ray and radio properties are described in Sects. 4 and 5. The statistical analysis of the radio to X–ray properties of the objects is given in Sects. 6 and 7.

2. The source sample

The objects studied in this paper were selected by a cross-correlation of a catalogue of radio sources at a flux density level above 15 mJy (for details see Neumann et al. 1994 (N94)) obtained from the Green Bank 5 GHz survey (Condon et al. 1989) of the northern sky $0^o \leq \delta_{1950} \leq +75^o$ and a source list obtained from the RASS (Voges 1992). The RASS was performed from August 1, 1990 to February 1, 1991 and yielded $\sim$ 50,000 X-ray sources with a positional accuracy such that 68% of the sources are found within $20''$ from their corresponding optical counterparts, and a limiting sensitivity of a few 10^{-13} erg cm^{-2} s^{-1} in the 0.1–2.4 keV energy band depending on the spectral form and the amount of Galactic absorption. It should be noted that the current data originate from the first processing of the RASS data as our follow–up observations started already during the final stages of the ROSAT Survey observations. Some inconsistencies in the flux density determination and inaccuracies in the positions, which do not affect the sample statistics, led later to a reprocessing of the data (RASS II, Voges et al. 1999) with improved quality.

We looked for correlations between the radio and the X–ray positions with angular distances of less than $100''$ and found a total of 2127 sources. For details of the source selection and the general properties of the sample see B95 and B97. To obtain accurate source positions and core radio fluxes, all objects were observed with the VLA in snap shot mode. The details and the results of these observations are presented in L97. For 1861 objects sub-arcsec positions and fluxes could be obtained, 436 sources were detected only at low resolution and in 72 fields no source was found with a signal-to-noise ratio greater than 5.

2.1. Optical and X–ray data

The optical and X–ray data listed in the tables were already presented and discussed in more detail in B95 and B97. New optical identifications have been made by L97. For previously optically identified sources we used the data as available from NED. For optically unidentified objects we determined plausible optical counterparts, using the accurate VLA positions (L97), from O and E POSS plates digitized with the Automatic Plate Measuring (APM) machine at $1.0''$ resolution. Usually, there is an optical object at distances less than a few arcsec from the VLA position, but for a small number of sources the closest optical object might be more than $20''$ away. For further analysis relying on the optical properties of the counterparts we will thus only take objects with separations of $\Delta \leq 4''$.

We obtained the X–ray fluxes from the measured count rates by assuming an average photon index of $\Gamma = 2.2$ for the underlying X-ray spectrum and Galactic absorption (Dickey & Lockman 1990, Stark et al. 1992; for details see Brinkmann et al. 1994). The stated errors merely reflect the errors in the counting statistics of the survey sources and do not incorporate deviations from the assumed power law slope, additional absorption, or systematic errors depending on the form of the local X–ray background and on details of the detection algorithm. Therefore, a total error of the X–ray flux of the order of $\lesssim 25\%$ must be regarded as a conservative estimate.

The quoted photon indices (assuming Galactic absorption) were estimated using the two hardness ratios given by the Rosat Standard Analysis System (Voges et al. 1999) by the method described in Brinkmann et al. (1994). The errors of the power law indices were estimated from the errors of the hardness ratios (Schartel 1995).

Boller et al. (1998) have correlated 120,000 ROSAT All-Sky Survey sources with 14,315 extragalactic IRAS sources and found a coincidence for 372 sources. Just three of them are included in our sample, namely 3C120, 3C273 and OJ 287 (RGBJ0854.8+2006), and therefore no infrared data are included in the tables.

3. Follow-up observations with the Effelsberg 100-m telescope

The radio sources showing up in the ROSAT All-Sky Survey are just a small fraction of all X–ray sources. It is therefore of interest to investigate their properties in more detail and to get an idea what makes them loud both in the X–ray and the radio range. We have used the 100-m telescope to quasi-simultaneously measure the flux densities of selected sources at 11 cm, 6 cm and 2.8 cm. These observations result in integrated flux densities, deconvolved sizes, linear percentage polarization and polarization angle of these sources.

A first sample of 234 radio sources has been studied in follow-up observations with the 100-m Effelsberg telescope to obtain contemporaneously measured radio spectra between 21 cm and 2.8 cm (N94). These sources have flux densities exceeding 20 mJy in the 5 GHz Green Bank survey source list. An analysis of these data shows that the properties of this sample,

when compared to those of radio sources without X–ray emission, are not much different in general. However, there might be a weak excess of flat spectrum sources and a higher fraction of unresolved sources. Cumulative source counts show that the sensitivity of the RASS is rather limited. Based on these results we decided to observe a larger number of sources, but limited follow-up observations with the 100-m telescope to sources stronger than 100 mJy at 6-cm wavelength.

Here we present the results after the completion of the program in which most of the RGB sources with integrated flux densities $>$ 100 mJy were studied at 11 cm, 6 cm and 2.8 cm wavelength. The sample originally consisted of 864 objects. We present the results for 741 sources in this paper. 103 sources from this sample have already been observed and analysed (N94) and are included with updated X-ray flux densities. A few sources from the sample serve as "standard" calibrators at the Effelsberg telescope like 3C138, 3C286 and others, which are in their majority strong 3C-sources. We have added flux densities for these and other steep spectrum sources from the compilation by Kühr et al. (1979, 1981) and the more recent work by Ott et al. (1994). We took the corresponding linear polarisation data from the catalogue of Tabara & Inoue (1980). Another small subsample of 25 sources, which have an EGRET identification or are candidates to be identified with γ-ray sources, have been monitored from 1991 until 1995/1996 with the 100-m telescope. The results of these observations have been published elsewhere (Reich et al. 1993; Reich et al. 1998). This monitoring program was started after the RASS had been completed. Therefore we have included the earliest measurements from this program, which are nearest in time to the ROSAT observation. There remain about 123 sources from the sample which have either not been observed because of limited observing time or the sources appear too much extended to be reliably measured by our observational method of orthogonal cross-scans. Some sources, however, are features of well known supernova remnants in the Galactic plane or HII-regions with bright exciting stars and are therefore excluded. Very few radio sources from the sample could not be detected at all.

3.1. The observations, calibration and data reduction

We used the 11 cm, 6 cm and 2.8 cm receivers installed in the secondary focus of the 100–m telescope to observe the selected sources by orthogonal cross-scans. The observations were carried out between 1990 and 1995. Most of the early observations were published by N94, where also the telescope and the receiver performance was described. In brief, the cooled receivers installed in the secondary focus of the telescope have system temperatures below 60 K and the telescope has a HPBW of $4\farcm3$ at 11 cm, $2\farcm4$ at 6 cm and $1\farcm2$ at 2.8 cm wavelength. At all wavelengths the Stokes parameters I, U and Q were measured simultaneously. 3C286 served as the main calibration source with assumed flux densities of 10.4 Jy, 7.5 Jy and 4.5 Jy at 11 cm, 6 cm and 2.8 cm wavelength respectively. Its linear polarization was taken to be 9.9%, 11.3% and 11.8% at the three wavelengths with a common polarization angle of 33°.

The method of observation was to carry out orthogonal scans in the horizontal system centered on the source position taken from the 5 GHz Green Bank Survey. The total length of the scans was $16'$ at 11 cm, $10'$ at 6 cm and $4\farcm5$ at 2.8 cm wavelength, respectively. In both directions (azimuth/elevation) two scans were taken moving the telescope forward and backward. In some observing periods small telescope tracking errors were noted, which resulted in a slight increase of the HPBW, when averaging the forward and backward scan. This effect was measured from observations of the calibration sources and was taken into account in the off-line analysis. The length of the scans limits a determination of an accurate integrated flux density to Gaussian shaped sources to about $6'$ at 11 cm, $4'$ at 6 cm and and $2'$ at 2.8 cm wavelength. Larger sources require two-dimensional mapping, which needs more observing time than doing cross-scans and was not possible within this observing project.

Measurements of a source started at 11 cm, where pointing or position errors have the smallest effect. With the corrected position the 6 cm and subsequent 2.8 cm observations were carried out. In cases where position errors exceed 10% of the HPBW the observations were repeated. The measurement of one source at all three frequencies takes about 20 to 30 minutes, which we regard as a quasi–simultaneous observation. In some cases, where data were rejected in the reduction stage, repetitions were made and combined with measurements from the previous epoch. The epoch of each individual measurement is included in the tables.

The cross–scans were analysed by fitting a Gaussian to the averaged scans for each direction and peak flux densities were calculated by taking residual positional errors into account. The accuracy of the fit was never limited by noise, but occasionally by interference, baseline distortions by weather effects or confusion by unrelated sources or emission in the vicinity. All these effects required some correction to the standard result. From the fits we also derived the deconvolved Gaussian shape size of the sources. We calculated the integrated flux density and the source size in the equatorial system. As in N94 errors are classified in the tables. Spectral indices were subsequently calculated for the 11 cm/6 cm data, 6 cm/2.8 cm data and a single power law index was fitted to the three integrated flux densities.

Percentage polarizations at the three wavelengths were calculated using peak intensities in I, U and Q from the averaged scans of both observing directions. In addition we calculated the polarization angle in the equatorial system. Some uncertainties were introduced by the residual instrumental polarization, which are at about 1% or below of the total intensity. For weak sources having a low percentage polarization the signal-to-noise ratio in U and Q is small in particular at 11 cm wavelength and interference was often more severe than for the total intensity signals. We therefore limited all polarization results to measurements where the percentage polarization is 3% or above.

Sample page of Table 1.

```
RGBJ0006.4+1235    234     198     153   -0.29   0.19  0.1435E-13
0003+1219            1       1       1   -0.32   0.13  0.6096E-12
 0.9800 17.60       PL      PL      PL   -0.31   0.08  2.0 0.4 36
 QSO             8/  1     < 3   4/165  93.02 93.02 93.02    5.50
.....................................................................
RGBJ0006.0+1609    495     341     248   -0.66   0.19  0.2493E-13
0003+1553 N          1       1       1   -0.40   0.13  0.7388E-11
 0.4500 16.40       PL      PL      PL   -0.50   0.08  2.4 0.4  9
 QSO 4C +15.01     < 3     < 4     < 3  90.79 90.79 90.79    3.72
.....................................................................
RGBJ0006.0+3820    625     679     593    0.15   0.19  0.4995E-13
0003+3804            1       1       1   -0.17   0.13  0.7540E-12
 0.2290 19.40   58x 59  37x 33      PL   -0.05   0.08  -   -   41
 QSO S4 0003+38  4/ 72     < 3     < 3  93.54 93.54 93.54    7.08
.....................................................................
RGBJ0010.5+1058    216     254     456    0.29   0.19  0.2565E-13
0007+1041 N          1       1       1    0.73   0.13  0.1280E-10
 0.0872 15.40       PL      PL      PL    0.56   0.08  1.6 0.2  7
 QSO MRK 1501      < 9     <10     < 3  90.79 90.79 90.79    5.75
.....................................................................
RGBJ0010.5+4412    144     138     115   -0.08   0.26  0.1012E-13
0007+4355            1       2       2   -0.23   0.22  0.1366E-11
                 69x 91      PL  34x 34   -0.17   0.11  3.3 1.6 30
                  9/ 91  16/108   6/106  94.08 94.08 94.08    8.91
.....................................................................
RGBJ0013.5+4051   1231    1054     952   -0.27   0.19  0.8100E-13
0010+4034            1       1       1   -0.13   0.13  0.1697E-11
 0.2550 17.90       PL      PL      PL   -0.18   0.08  2.5 0.9 23
 G                 < 3     < 3     < 3  92.31 92.31 92.31    7.76
.....................................................................
RGBJ0017.7+7212    235     131      65   -1.03   0.19  0.8773E-14
0014+7155 N          1       1       2   -0.88   0.18  0.1210E-11
                    PL      PL      PL   -0.94   0.11  -   -   33
                   < 5     < 5       5  91.07 91.07 91.07    1.88
.....................................................................
RGBJ0017.7+0827    164      79      61   -1.29   0.26  0.6280E-14
0015+0811            1       2       3   -0.32   0.29  0.9027E-12
               119x 69  65x 27  63x 26   -0.70   0.15  1.8 0.9 32
                    -       -       -  93.54 93.54 93.54    5.01
.....................................................................
RGBJ0019.7+2602    579     534     427   -0.14   0.19  0.3873E-13
0017+2545            1       1       1   -0.28   0.13  0.4259E-11
 0.2840 15.40       PL      PL      PL   -0.23   0.08  2.7 0.3 13
 QSO 4C +25.01     < 3     < 3     < 3  92.49 92.49 92.49    3.72
.....................................................................
RGBJ0020.3+5918    214     174       -   -0.37   0.31  0.1252E-13
0017+5900            2       2       -    -      -     0.1994E-11
 -.0011 11.80  174x102 106x128       -    -      -     3.2 2.0 32
 G   UGC 00192   5/115     < 3       -  94.99 94.99    -    54.95
.....................................................................
RGBJ0022.1+4525    423     340     273   -0.39   0.19  0.2518E-13
0019+4508            1       1       1   -0.28   0.13  0.5887E-12
               90x100      PL      PL   -0.32   0.08  -   -   37
                3/ 25     < 3   3/ 77  93.64 93.64 93.64    8.32
.....................................................................
RGBJ0035.9+1553    267     161      80   -0.89   0.19  0.1062E-13
0033+1537            1       1       1   -0.88   0.13  0.5429E-12
 1.1600 18.00       PL      PL      PL   -0.88   0.08  1.8 0.8 39
 QSO               < 3   9/ 25  15/ 32  93.02 93.02 93.02    4.07
.....................................................................
RGBJ0036.1+1838   1076     572     246   -1.11   0.19  0.3710E-13
0033+1821            1       1       1   -1.06   0.13  0.5640E-12
 1.4690 20.00   53x 72      PL  23x 22   -1.08   0.08  1.7 0.8 38
 QSO 3C 014      4/ 84   4/ 77   8/ 75  92.49 92.49 92.49    4.07
.....................................................................
```

3.2. The tabulated results

In Table 1 we list the results of the radio observations together with the ROSAT X–ray data and optical identification as far as available. We only present a sample page of the table here; a full copy of the tables is available from the CDS via anonymous ftp to cdsarc.u-strasbg.fr. The VLA data of the souces are given in L97; all other available X-ray data are from B95 and B97.

Row 1 gives the Green-Bank identification and position of the radio source for epoch 2000, followed by 11 cm, 6 cm and 2.8 cm integrated flux densities (mJy/beam area). The spectral index α defined by $S \sim \nu^{\alpha}$ for the 11 cm and 6 cm flux densities and its error. The last entry is the radio frequency integrated flux density (erg cm^{-2} s^{-1} for the frequency band from 2.695 GHz to 10.45 GHz).

Row 2 gives the position for epoch 1950. A letter N refers to N94, where the radio measurements originate, but the X–ray flux densities are revised. K and O indicate that flux densities are taken from Kühr et al. (1979, 1981) or from Ott et al. (1994) and polarization data are from Tabara & Inoue (1980). The error class for the 11 cm, 6 cm and 2.8 cm integrated flux densities are the next three entries. The error classes are defined by 1 $\equiv \ \leq 9\%$ error, 2 $\equiv \ \leq 14\%$ error, 3 $\equiv \ \leq 23\%$ error and 4 $\equiv \ \geq 23\%$ error. The spectral index 6 cm/2.8 cm and its error comes next. The final entry is the X–ray energy integrated flux density (erg cm^{-2} s^{-1}) in the 0.1 - 2.4 keV energy range.

Row 3 gives the measured redshift z followed by the optical magnitude (V in most cases), the deconvolved source sizes along right ascension and declination at 11 cm, 6 cm and 2.8 cm, respectively. PL denotes "pointlike" sources having deconvolved sizes of up to 56″, 40″, 16″ in one or both coordinates at 11 cm, 6 cm and 2.8 cm, respectively. It follows the spectral index resulting from a fit of the spectrum between 11 cm and 2.8 cm wavelength and its error. The last three entries are the X–ray power law photon index, its error and the percentage error of the X–ray flux density.

Row 4 gives an optical identification or a common source name taken from B95 if available. G stands for galaxy, QSO for a quasar, BLL for a BL Lac type object and GCL for a galaxy cluster. The following three or six entries are the percentage polarization and the polarization angle for 11 cm, 6 cm and 2.8 cm. For the measurements taken from N94 only percentage polarizations are given. For percentage polarizations of less than 3% no polarization angle is given. The epoch of observation at the three wavelengths follows next and the final entry is the column density of neutral hydrogen $N_{\rm H}$ in units of 10^{21} cm^{-2}.

Table 2 lists 57 additional observations from 48 sources, which were observed more than once. These data are indicative for possible variability. The observations listed in Table 2 always have later epochs than those given in Table 1. The layout of Table 2 and Table 1 is identical.

3.3. Source statistics and optical identification

For the 741 X–ray selected sources in Table 1 we list data for 697 sources at 11 cm, for 729 sources at 6 cm and 698 sources at 2.8 cm. Optical data are available for 468 sources or 63% of the sample. Due to the 100 mJy flux density limit at 6 cm the fraction of identified sources in the sample is two times larger than that for the entire sample of 2127 sources (B95). From the 468 optically identified sources 274 are quasars, 56 are BL Lacs, 116 are galaxies and 22 are clusters of galaxies. Redshifts are known for 405 sources and Fig. 1 shows their distribution. About 50% of the sources have redshifts below z = 0.5, while for 25 sources z is larger than 2.

4. The X-ray properties of the sample

Fig. 2 shows cumulative source counts of the X–ray sources. The slope of about -1 for flux densities exceeding about $5\,10^{-13}\,[\mathrm{erg\,cm^{-2}\,s^{-1}}]$ is unexpectedly flat and deviates greatly from the expected slope of -1.5 for a uniform source density without source evolution effects. This indicates strong selection effects. The sensitivity of the ROSAT survey varies according to the HI–column density as shown in Fig. 3, where detected X–

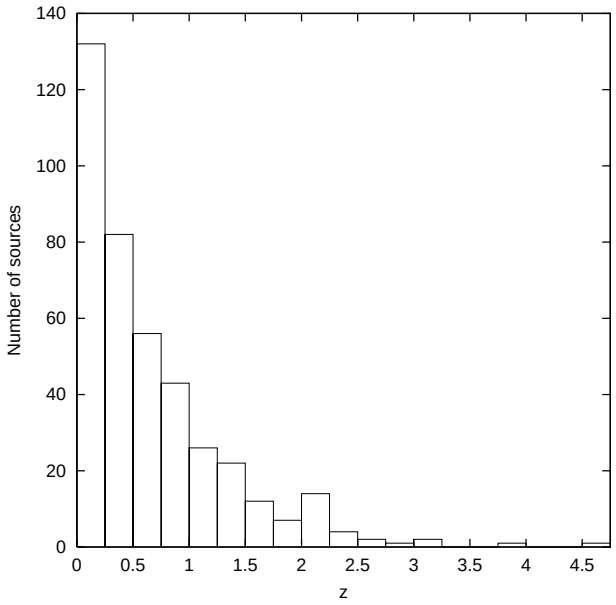

Fig. 1. Redshift distribution for 405 out of 741 sources of the sample.

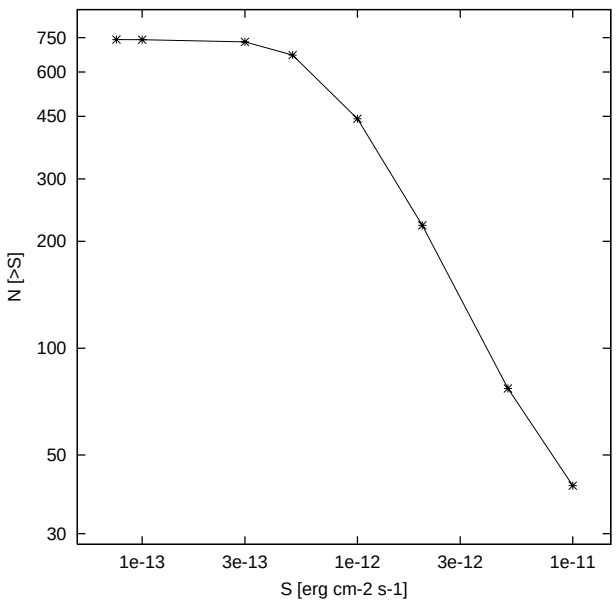

Fig. 2. Cumulative counts for 741 X-ray sources.

Table 3. Fitted mean HI column density and mean X–ray spectral index Γ from N sources versus Galactic latitude b.

b °	N	HI $[10^{21}\mathrm{cm}^{-2}]$	N	Γ
0–15	97	26.85	53	3.11
15–30	163	7.66	122	2.54
30–45	208	3.99	150	2.22
45–60	132	2.56	113	2.09
60–75	92	1.84	75	1.92
75–90	47	1.54	39	1.90

ray flux densities versus HI–column density are plotted. A clear and expected selection effect is apparent in the sense that weak X–ray sources are only detected when the HI–column density is sufficiently low. Since the HI–column density is highest close to the Galactic plane only strong sources are detected in that area (Table 3). In addition, the exposure of the survey varies and is largest at the ecliptical poles, where the HI–column density is small. These effects lead to a slightly inhomogeneous sample. Fig. 4 shows the average redshift z versus binned X–ray flux densities. The expected distribution for an unbiased uniform source sample is seen, where weaker sources are more distant on average than stronger ones.

The tables include the X–ray spectral indices, which are the power law slopes assuming Galactic absorption as described by B95 and B97. In Fig. 5 we show the distribution for 547 sources with spectral indices of up to 5 in the same way as B97, where a detailed discussion of spectral properties and distribution for various classes of objects has been given. 6 sources of our sample have spectral indices exceeding 5. Fig. 5 shows that the maximum number of sources is counted for the spectral range between 2.0 to 2.4. There is a slight excess of steep spectrum sources, as noted by B97 before, which is predominantly associated with unidentified sources. The spectral index

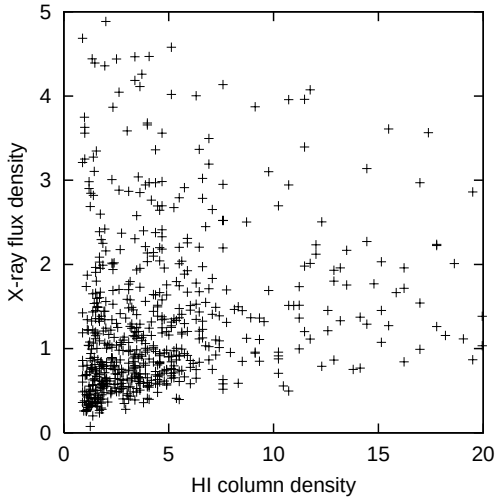

Fig. 3. HI column density $[10^{21}\mathrm{cm}^{-2}]$ versus X-ray flux density S_x $[10^{-12}\ \mathrm{erg\ cm^{-2}\ s^{-1}}]$.

is slightly dependent on the Galactic latitude b, which in turn depends on the HI–column density (Table 3). This effect was already discussed by B97, where it has been concluded that in general lower count rates towards the Galactic plane by increasing HI–absorption favour the detection of steep spectrum sources.

5. The radio properties of the sample

Fig. 6 shows the cumulative source counts at 11 cm, 6 cm and 2.8 cm, respectively. An increasing flattening from the expected slope of -1.5 for a uniform source distribution is seen for flux densities below about 1 Jy. This result was already noted for the radio samples discussed by N94 and B95 and indicates a selection effect of the radio source sample due to the limited sensitivity of the ROSAT survey.

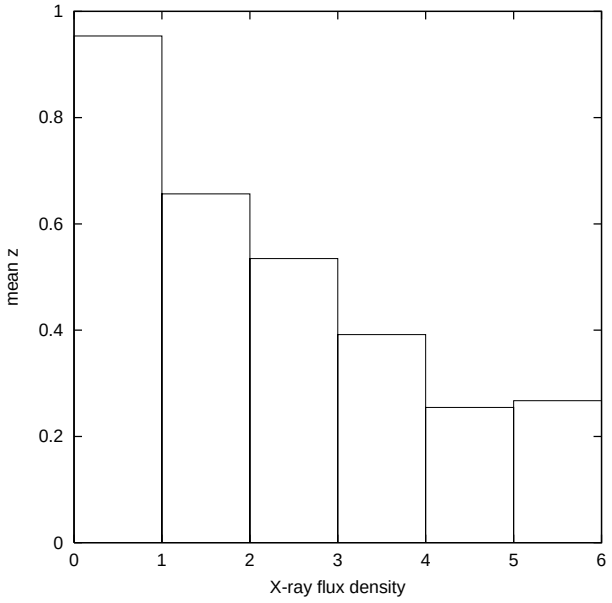

Fig. 4. Mean redshift versus X–ray flux density S_x [10^{-12} erg cm^{-2} s^{-1}].

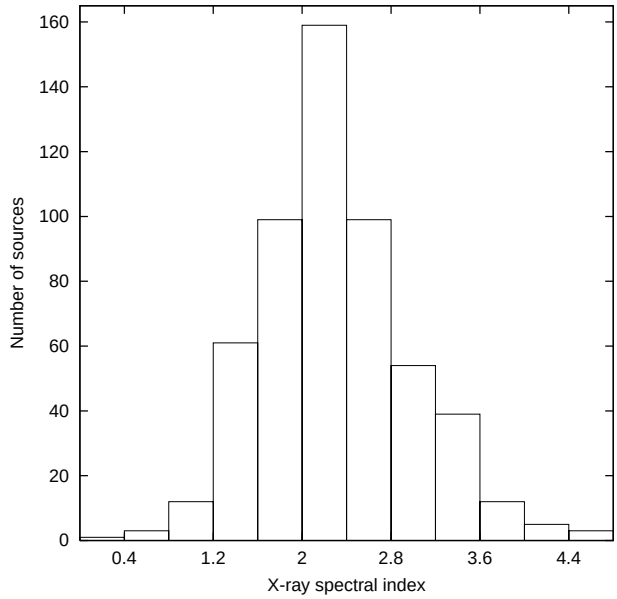

Fig. 5. Distribution of X–ray spectral indices.

Table 4. Mean z versus radio flux density at 11 cm, 6 cm and 2.8 cm for 100 mJy bins below a flux density of 500 mJy and 500 mJy bins above. N is the number of sources per bin.

S[mJy]	N(11)	z(11)	N(6)	z(6)	N(2.8)	z(2.8)
150	36	0.32	68	0.48	81	0.54
250	48	0.45	60	0.55	55	0.66
350	40	0.73	45	0.55	32	0.65
450	38	0.59	26	0.70	30	0.67
750	101	0.76	93	0.81	65	0.84
1250	49	0.83	40	0.87	25	1.11
1750	26	0.81	16	0.95	23	0.98

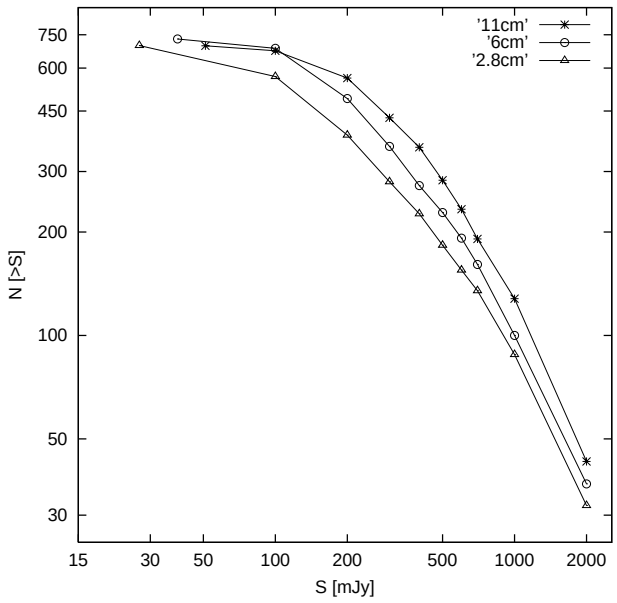

Fig. 6. Cumulative source counts at 11 cm, 6 cm and 2.8 cm wavelength.

As already noted by N94 the X–ray selected radio sources are more compact than those from an unbiased sample. N94 find 81%, 76% and 69% of sources unresolved at 11 cm, 6 cm and 2.8 cm, respectively. The present sample, which is about three times larger and includes the N94 sources gives 66%, 71% and 67%, respectively, for the three wavelengths. An unbiased source sample taken from the Condon et al. 6 cm survey shows just 52% sources to be unresolved. The beam size of this 6 cm survey is close to that of our 11 cm beam. We consider the higher fraction of compact radio sources in the X–ray selected sample as significant.

Table 4 shows the mean redshift versus flux density at 11 cm, 6 cm and 2.8 cm. Comparing Table 4 with Fig. 4, where the X–ray flux density versus mean z is shown, a significant difference is noted. For stronger radio sources the average redshift z increases. Such a behaviour is expected when more and more weaker sources are included in an unbiased sample. This result indicates that the X–ray selected radio sources contain more luminous radio sources or sources where directed emission contributes more to the total flux density than for an unbiased radio sample.

Fig. 7 shows the three radio spectral index distributions as listed in Tables 1 and 2. In N94 we have compared the spectral index distribution 11 cm/6 cm with the distribution derived from two radio surveys at 11 cm (Loiseau et al. 1988) and at 6 cm (Condon et al. 1989) and found about 9% more sources with spectral indices $\alpha > -0.6$. Fig. 8 shows the distribution for the present sample, which corresponds to Fig. 2 in N94. The same excess of about 9% of flat spectrum sources is noted, if compared with the unbiased radio sample. However, the present sample consists of stronger sources than the N94 and the Loiseau et al. sample. In addition, as we have listed in Table 5, there is a clear dependence of the average spectral index on the flux density in

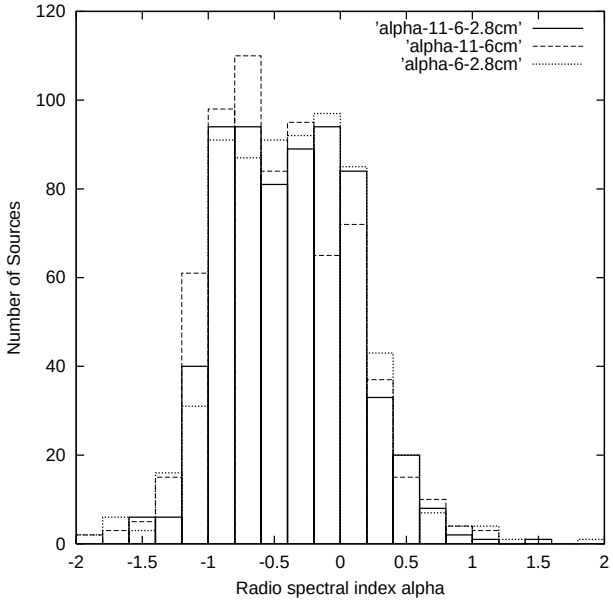

Fig. 7. Distribution of radio spectral indices for the long and short wavelengths and the spectral fit from the data of all three wavelengths.

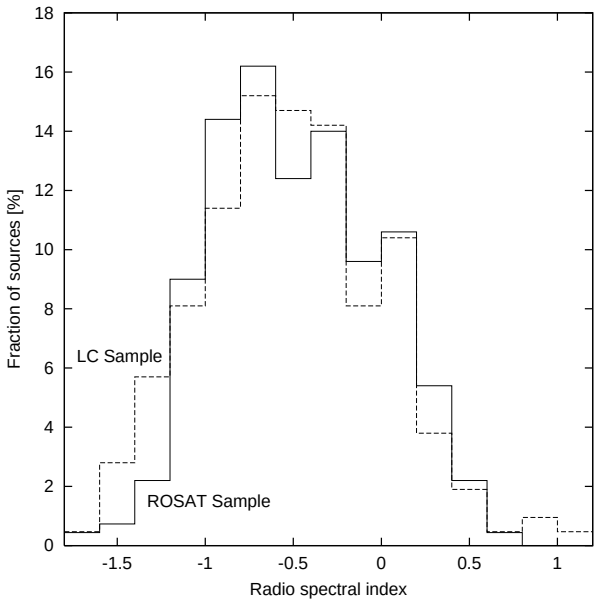

Fig. 8. Fractional distribution of radio spectral indices of the ROSAT selected sources and the Loiseau et al. / Condon sample. Both distributions are for spectral indices from 11 cm to 6 cm wavelength.

the sense that stronger sources show flatter spectra. This result is in accordance with the increase of the mean redshift with flux density (Table 4), which can be understood as the result of a contribution from beamed radio emission emerging from the core. This emission is known to show flatter spectral indices if compared to the total emission of extragalactic sources. We have also checked our spectral index distribution for a dependence on the redshift as listed in Table 6. Sources with steep spectra have a smaller redshift than flat or inverted spectrum sources.

Table 5. Dependence of spectral index on 6 cm flux density.

S 6cm (Jy)	N	α 11-6-2.8cm	N	α 11-6cm	N	α 6-2.8cm
$<$0.5	430	-0.44	499	-0.49	499	-0.39
0.5-1	122	-0.27	129	-0.24	129	-0.29
$>$1	91	-0.23	98	-0.24	99	-0.21

Table 6. Mean z and its dispersion σ(z) versus binned radio spectral indices α(11-6-2.8 cm). N is the number of sources per bin.

α	N	z	σ(z)
-1.5 - -0.9	55	0.43	0.06
-0.9 - -0.3	168	0.55	0.05
-0.3 - 0.3	120	0.88	0.06
0.3 - 0.9	20	0.84	0.20
0.9 - 1.5	5	1.04	0.28

Table 7. Mean absolute spectral differences dα for sources with spectral indices in the NED data base and the Effelsberg spectral indices versus the binned Effelsberg spectral indices α. N is the number of sources and $\sigma(\alpha)$ the dispersion of dα.

α	N	dα	$\sigma(\alpha)$
-1.2 - -0.9	17	0.14	0.03
-0.9 - -0.6	36	0.10	0.01
-0.6 - -0.3	27	0.19	0.02
-0.3 - 0.0	34	0.24	0.03
0.0 - 0.3	25	0.22	0.04
0.3 - 0.6	10	0.54	0.11

The difference for all sources with spectral indices above and below α = -0.3 is Δz = 0.36.

We have compared our spectral indices with those listed in the NED database and show the result of this comparison in Table 7. On average our simultaneous observations result in spectral indices which deviate from the NED data by about 0.1 to 0.2, except for sources with an inverted spectrum. Here the mean difference increases significantly to about $\Delta\,\alpha = 0.5$ for sources with $\alpha > +0.3$. Variability of an active core is the most likely reason for this result, which is quite often accompanied by spectral changes. However, spectra of variable sources calculated from non–contemporary data might also be present in the NED database and result in large differences. Depending on the time scale of variability spectra from non–contemporary data are mostly meaningless. Radio flares often evolve by showing up first at high frequencies and inverted spectra are seen. Later the source becomes optically thin at longer wavelength as well and the spectrum steepens. The frequency of occurence of radio flares is known to differ largely for AGN. It must be noted at this point that the observed X–ray flux densities are not contemporarily measured with our radio data and therefore any related variability is lost.

Table 8 lists the distribution of the percentage polarization at the three wavelengths. As stated in Sect. 3.1 we only give the

Table 8. Distribution of percentage linear polarization PC at 11 cm, 6 cm and 2.8 cm wavelength.

PC	N(11cm)	N(6cm)	N(2.8cm)
3	44	77	85
4	55	67	69
5	44	56	55
6	32	55	34
7	22	28	20
8	22	19	24
9	21	15	14
10	9	7	12
11	3	8	11
12	2	3	3
13	3	4	5
14	3	4	2
>15	3	2	6

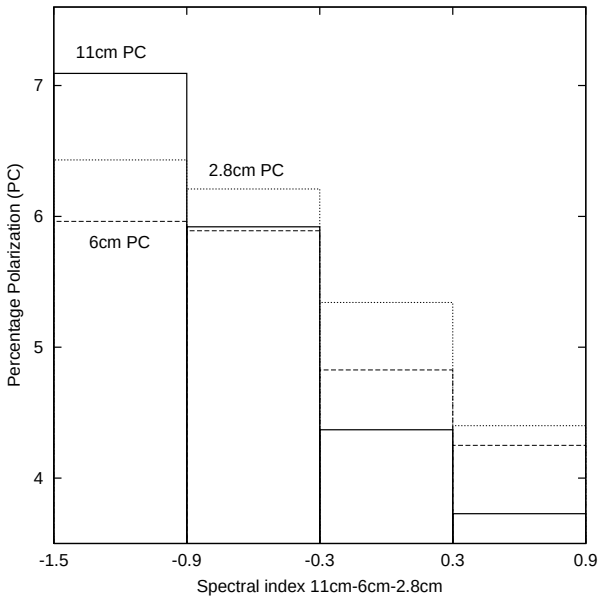

Fig. 9. Dependence of the percentage linear polarization at 11 cm, 6 cm and 2.8 cm wavelength versus binned radio spectral indices.

results for sources with the percentage polarization $\geq$3%, where any disturbing instrumental influence can be ignored. Omitting sources with no or disturbed polarization data we count 578 sources at 11 cm of which 263 are polarized. From 684 sources at 6 cm 345 are polarized and at 2.8 cm we list 340 out of 674 sources. This corresponds to a fraction of 45% at 11 cm, 50% at 6 cm and 2.8 cm of sources with more than 3% polarization. There is no significant difference in the distribution of percentage polarization with wavelength (Table 8). If internal source depolarization is important one would expect more polarized sources and a higher degree of polarization for the high frequency data.

As stated in N94 it is difficult to find unbiased source samples for comparison. The two samples at 10 GHz by Okudaira et al. (1993) for flat spectrum sources show 30% and that of Simard-Normandin et al. (1982) for known polarized sources 43% of sources with linear polarization exceeding 3%. It seems that the X–ray selected radio source sample is slightly higher polarized than otherwise selected source samples, an effect which has to be quantified more precisely.

A dependence of the percentage polarization on the spectral index is obvious from Fig. 9. Higher percentage polarization on average is noted for steep spectrum sources. We find no significant dependence of the percentage polarization for any of the three wavelengths on the redshift.

A sample of 154 extragalactic sources, which were previously known to be polarized, have been observed by Zukowski et al. (1999) at 6 cm wavelength with the 100-m telescope. Zukowski et al. find about 71 sources or 46% to be polarized by more than 3%. This fraction is similar to our fraction of 50% polarized sources. However, a significant difference between the source samples is noted when comparing the number of polarized sources for z < 0.5 with those for z > 0.5. The Zukowski et al. sample results in 30/19 sources, while our sample of X–ray selected radio sources has 94/99 sources for z below and above 0.5. The sample of Zukowski et al. largely consists of sources from the 3C or 4C–catalogues, which are less distant and have in general higher flux densities than the sources of the X–ray selected sample. It was already noted that for this sample the strong radio sources have on average higher z values than the weak sources. The distribution of percentage polarization for sources above and below z = 0.5 is very similar. This means that the redshifted sources are on average not higher polarized than the local ones in accordance with the general distribution of polarization for our sample (Table 8).

5.1. Rotation measures

We have calculated rotation measures (RMs) from the measured polarization angles ϕ_λ, with ϕ_λ = RM λ^2 + ϕ_0, where ϕ is measured in radian, λ in m and RM in radian/m^2. We will use data from 291 sources in the further analysis. It is well known that at least three frequencies are required to determine a RM free from ambiguity (+/- π). However, we have also added RMs derived from polarization data available at just two frequencies. In the case of combining 11 cm/6 cm data and 6 cm/2.8 cm data the ambiguity is 813 $\mathrm{rad\ m^{-2}}$ or 988 $\mathrm{rad\ m^{-2}}$, respectively. In most cases these large ambiguities are beyond the expected values of RM. A smaller ambiguity of 262 $\mathrm{rad\ m^{-2}}$ exists, when combining 11 cm/2.8 cm data, which makes a correct RM–value more uncertain. However, this case holds just for a small group of polarized sources. For the subsequent analysis we use absolute values of RM.

Fig. 10 shows the distribution of RM versus Galactic latitude and for comparison the RM distribution from the Simard-Normandin et al. (1981) sample (SKB–sample) of 555 sources. These RMs were calculated based on various polarization surveys of extragalactic sources. Both distributions quite clearly show an excess of RMs close to the Galactic plane. This increase is certainly caused by the magneto–ionic medium of the Galactic disk. Apart from this effect there is a systematic ex-

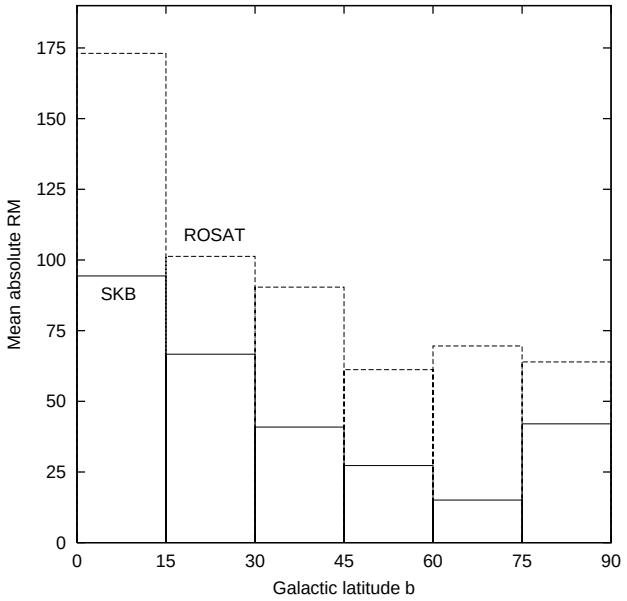

Fig. 10. Mean absolute rotation measure RM [rad m^{-2}] versus Galactic latitude. The ROSAT selected sample is compared with the unbiased sample of Simard-Normandin et al. (1981) (SKB).

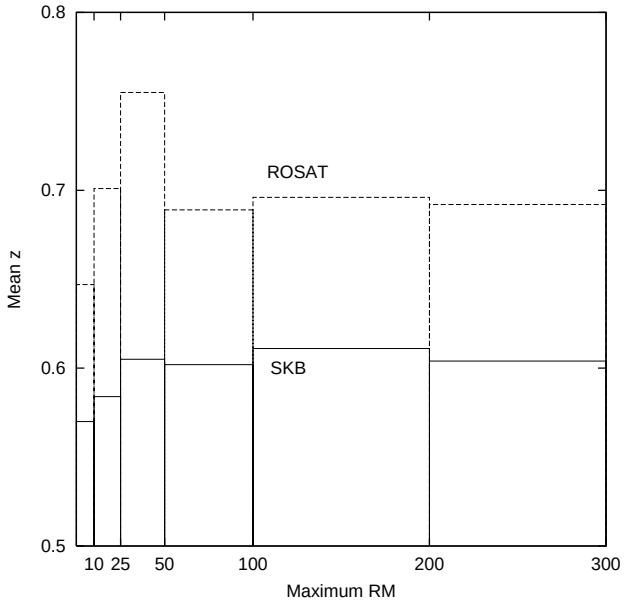

Fig. 11. Mean redshift z of all sources with rotation measures RM [rad m^{-2}] up to the maximum value.

cess for all Galactic latitudes of the average RM for the X–ray selected radio sources, if compared to the SKB–sample of polarized radio sources. Excluding the sources below a Galactic latitude of 15°, where the X–ray sample is rather incomplete and the number of sources is small, we find an excess of 44 $\mathrm{rad\ m}^{-2}$. The average for all sources is 49 $\mathrm{rad\ m}^{-2}$ for the SKB–sample and 93 $\mathrm{rad\ m}^{-2}$ for the X–ray selected sample.

Fig. 11 shows the average redshift versus cumulative RMs for both samples. While the average z decreases for RMs below

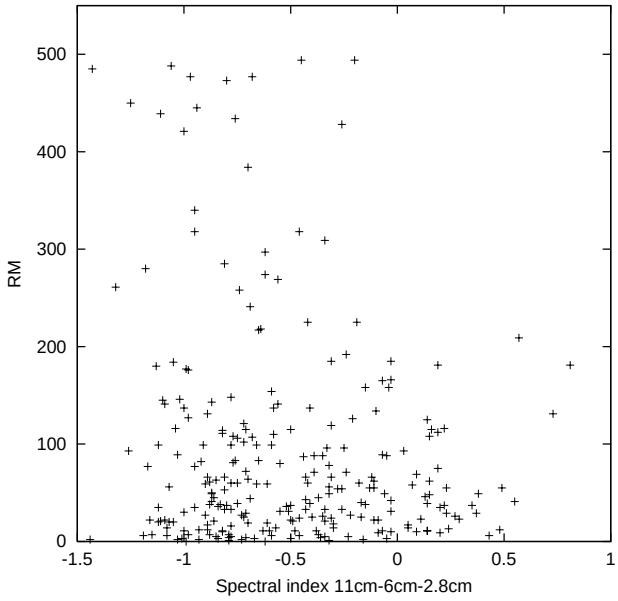

Fig. 12. Absolute rotation measure RM [rad m^{-2}] versus radio spectral index.

Table 9. Mean absolute rotation measure RM versus radio spectral index.

α 11-6-2.8cm	N	RM [rad m^{-2}]
-1.4 - -1.0	20	101
-1.0 - -0.6	66	94
-0.6 - -0.2	45	98
-0.2 - 0.2	34	63
0.2 - 0.6	11	43

$10\,\mathrm{rad\ m}^{-2}$ for both data sets, the X–ray selected sample always has slightly higher z values of about 0.09 for all RM-intervals.

Comparing RM and redshift one has to take into account where the RM originates. Certainly there are Galactic contributions and in addition contributions from intervening halos of galaxies or galaxy cluster. For the case that the RM entirely originates at the source it needs to be scaled by $(1+\mathrm{z})^2$, resulting from the λ^2 dependence of RM and the redshifted observing wavelength. An average increase of the redshift from about 0.6 for the SKB–sample to about z = 0.7 for our sample means an increase of RM by up to 1.13, but a factor of 1.9 is observed. Because of RM $\sim\ \mathrm{B}_{||}\,\mathrm{n_e}\,l$ this is an indication that an additional or stronger magnetic field component $\mathrm{B}_{||}$ in the line of sight l exists or, as an alternative, an enhanced electron density $\mathrm{n_e}$ is causing the systematic increase of RM in the X–ray selected sample.

Welter et al. (1994) have investigated the RM dependence of z for a quasar sample to check the intrinsic origin of the RM. Their data show for redshift corrected RMs a factor of 4 between the RMs for sources with z = 2 and z = 0.5. We calculate about the same factor for the quasars in our sample, although the number of quasars with RM exceeding z = 1.75 is just 8.

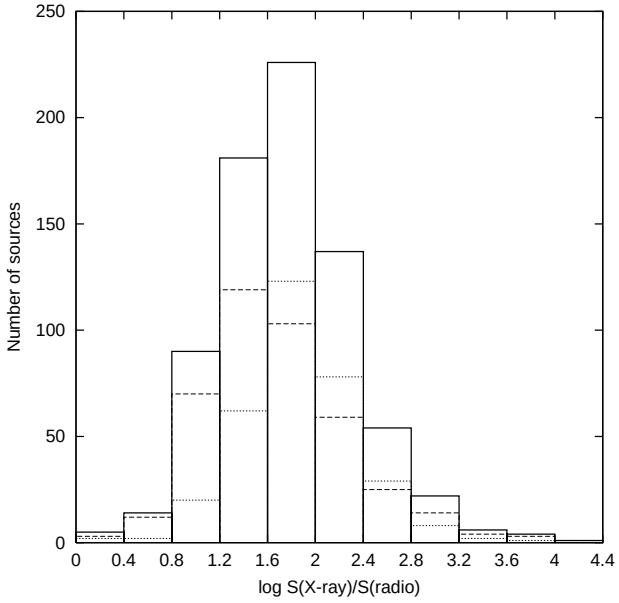

Fig. 13. Distribution of the ratio of the X-ray to radio flux densities for all sources, 413 flat spectrum radio sources (α > -0.5, long dashes) and 328 steep spectrum radio sources (α < -0.5, dotted).

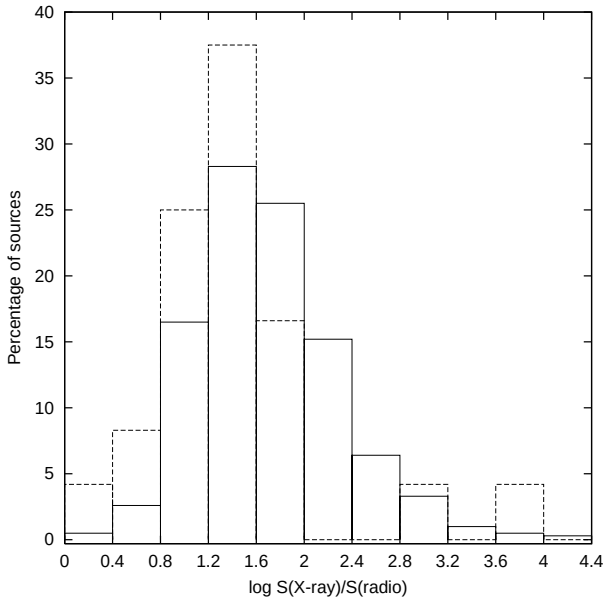

Fig. 14. Distribution of the ratio of the X-ray to radio flux densities for flat spectrum radio sources (α > -0.5, full line) and flat spectrum EGRET sources including candidate sources (dashed).

Table 10. Average absolute rotation measure RM for unresolved (PL) and extended (EX) sources at the three observing wavelengths.

λ (cm)	N (PL)	RM (PL) ($\mathrm{rad\ m^{-2}}$)	N (EX)	RM (EX) ($\mathrm{rad\ m^{-2}}$)
11	157	88	105	111
6	179	86	96	118
2.8	158	93	108	104

Fig. 12 shows the distribution of RM versus the radio spectral index α. It is quite obvious that only a few sources with flat or inverted spectra have large RMs. In Table 9 we list the binned distribution with a clear decrease of RM with increasing spectral index. It should be noted that 131 sources have spectral indices $\alpha < -0.2$, while 45 sources have larger spectral indices. Despite the different number of sources we think the result is significant.

We have also looked at a possible dependence of the RM versus the mean diameter of the source. Table 10 lists the result. The data indicate a slightly larger RM of about 10 - 30 $\mathrm{rad\ m^{-2}}$ for the resolved sources (EX in Table 10) compared to unresolved (PL) sources.

6. Correlation of the radio and X–ray data

6.1. Flux densities

The distribution of frequency-integrated radio and X–ray flux densities for our sample of 741 sources is rather similar to that of N94, where 211 sources are shown, although the weak radio sources are missing in the present sample.

Fig. 13 shows the ratio of the X–ray to radio flux densities. The mean ratio of the total sample is smaller, if compared to N94 (Fig. 7) due to the higher radio flux densities studied here. The difference in the distributions of steep and flat spectrum radio sources is about the same as for the N94 sample. If we compare the ratios of X–ray to radio flux densities for flat spectrum sources and those for the 24 flat spectrum identified or candidate EGRET sources (in total these are 25 sources) as shown normalized in Fig. 14, we see a further trend towards smaller ratios for the γ–ray sources. No γ–ray source is seen in the log S(X–ray)/S(radio) interval between 2.0 and 2.8. However, two sources are exceptional in this small sub-sample, which show additional TeV–emission, namely MKN 421 (Punch et al. 1992) and MKN 501 (Quinn et al. 1996; Atkins et al. 1999). They have unusual high flux density ratios of 2.85 and 3.86. This is in accordance with the BL Lac characteristics of these objects with very small viewing angles and a synchrotron spectral energy distribution peaking in the soft to medium X–ray range. The TeV and γ-ray emission is likely inverse Compton scattered emission from the synchrotron emitting electrons.

The present sample contains 320 sources with a radio spectral index α > -0.3 compared to 40 sources as observed by N94. When relating the frequency-integrated radio versus X–ray flux densities N94 noted an apparent clustering of the source distribution into two subgroups (N94, Fig. 8). This effect, however, is smoothed out in the present much larger source sample as shown in Fig. 15. The distribution for the steep spectrum and curved spectrum sources for the present larger sample is similar to that of N94 (Figs. 9 and 10), although the scatter is larger now. We conclude, that there are no apparent indications for a relation between the radio and X–ray flux densities.

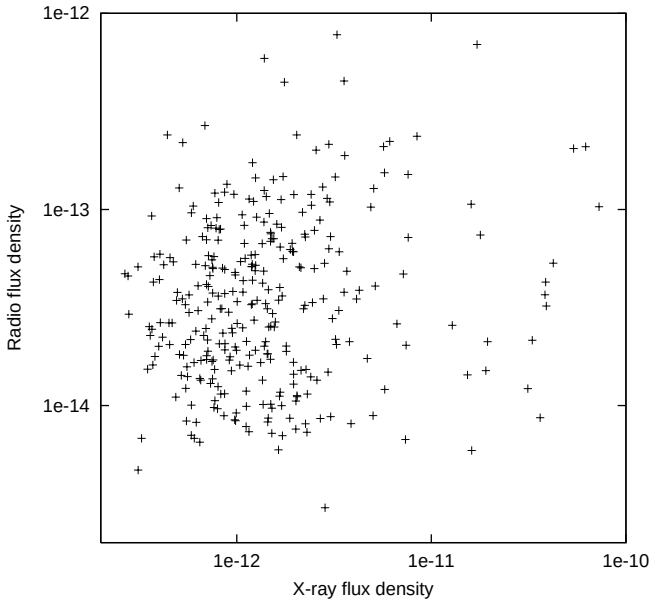

Fig. 15. Integrated X-ray flux densities versus integrated radio flux densities for flat spectrum sources.

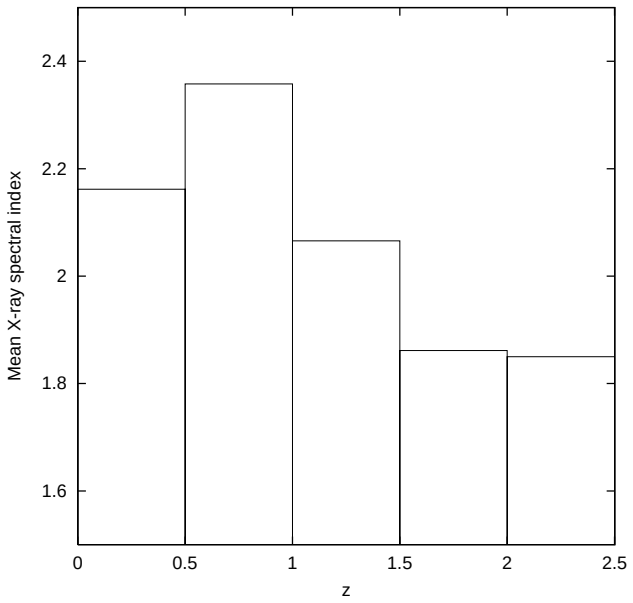

Fig. 17. Mean X-ray spectral index versus redshift z.

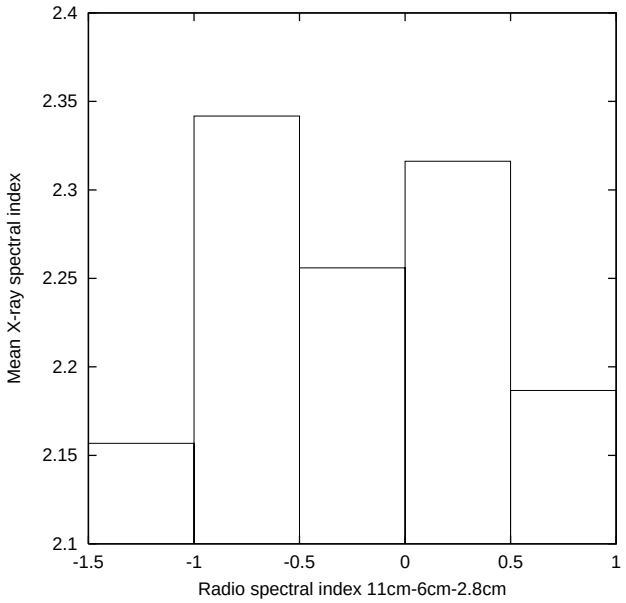

Fig. 16. Radio versus X-ray spectral indices.

6.2. Spectral indices

We have looked for a dependence of the radio spectral indices with the X–ray spectral indices. Fig. 16 displays the result for 487 sources. A variation of the X–ray spectral index between 2.25 and 2.35 for radio spectral indices between -1 and 0.5 is seen, while the sources with steeper or flatter radio spectra both have X–ray spectral indices below 2.2. Siebert et al. (1998) found for a sample of flat spectrum Parkes radio sources with $\alpha > -0.5$ a systematic hardening of the X–ray spectral index with increasing radio spectral index, while Fig. 16 indicates just a hardening for inverted radio spectra with $\alpha > 0.5$. Siebert et al. (1998) explain this effect as a consequence of unification schemes, where an increasing fraction of beamed X–ray emission is expected for radio sources with a dominating beamed component. The same effect of spectral hardening, however, is also seen for very steep spectrum radio sources, which in their majority are identified with radio galaxies. Galaxies as a group are known to have harder X–ray spectra than quasars and BL Lac objects (B97, Siebert et al. 1998).

The average radio spectral index does not vary significantly for the 486 X–ray spectral indices ranging up to 4.5. For X–ray spectral bins of 1 the radio spectral index varies between -0.33 and -0.47. The 5 sources with X-ray spectral indices between 4.5 and 5.5, however, have α = -0.75.

For 229 sources with X-ray spectral indices we have calculated RMs. About 166 of those sources have RM $< 100\,\mathrm{rad\,m^{-2}}$ with an average X-ray spectral index of 2.24. The 63 sources with RM $> 100\ \mathrm{rad\ m^{-2}}$ have an index of 2.62 on average. As shown above both parameters depend on Galactic latitude or HI–column density and this is reflected in the increase of the X–ray spectral index with RM.

The dependence of the X–ray spectral index on redshift was already discussed by Siebert et al. (1998). A hardening with z is expected because flat spectrum emission at high energies is shifted into the ROSAT band. In addition, the soft steep spectrum sources are shifted to low frequencies outside of the observing band. The observed mean X–ray spectral index distribution versus redshift is shown for 304 sources in Fig. 17. A spectral flattening with increasing redshift is seen. This dependence is the same as found by Brinkmann et al. (1997a) and Siebert et al. (1998) for quasar samples. For 25 sources with z > 2 the spectral index is close to 1.85. The 168 sources with redshifts below z = 0.5, however, have a flatter spectrum than the 76 sources with z = 0.5 to z = 1. At low redshifts the fraction of galaxies increases, which have on average flatter spectra than quasars.

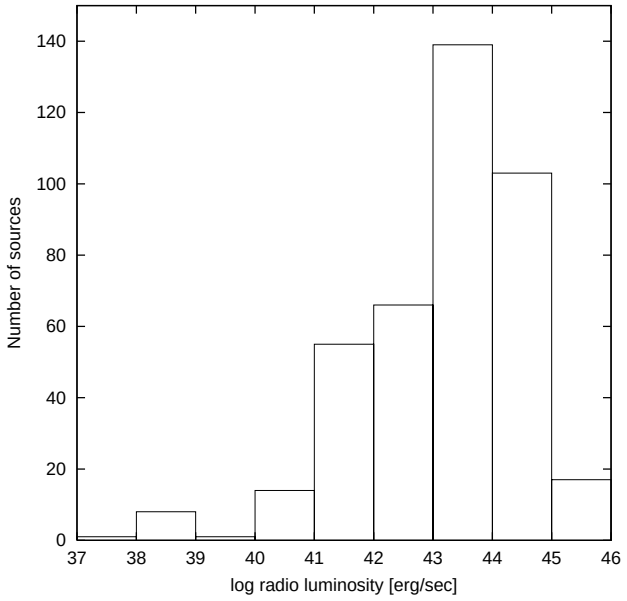

Fig. 18. Distribution of radio luminosities L_r.

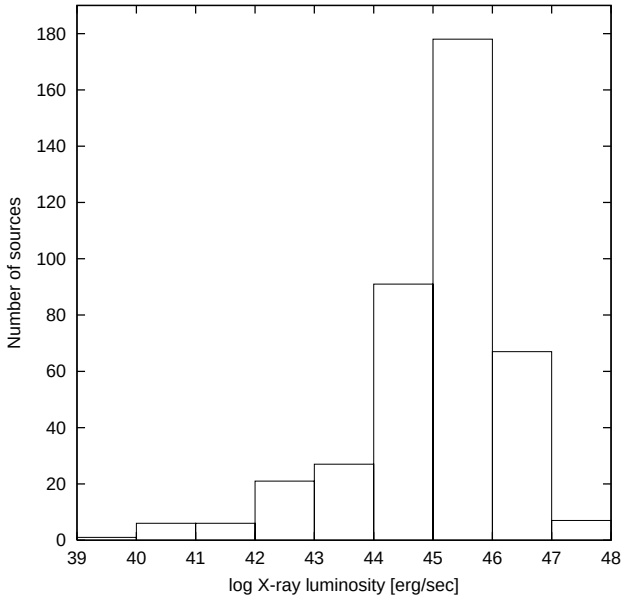

Fig. 19. Distribution of X-ray luminosities L_x.

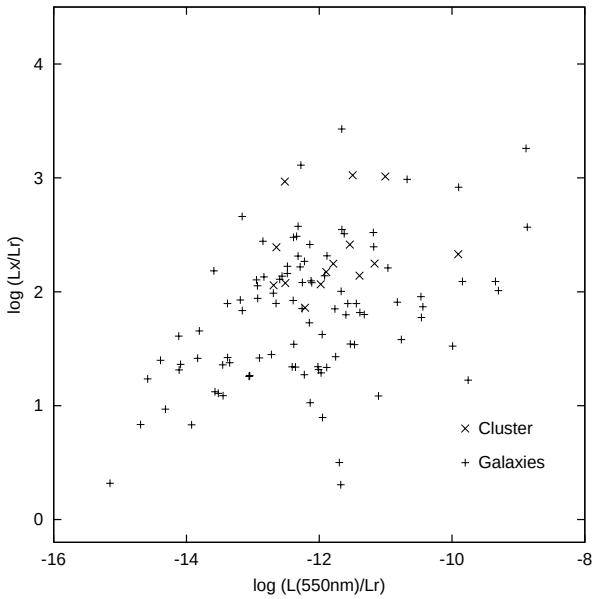

Fig. 20. The luminosity ratios of X-ray and radio emission versus the ratios of optical and radio emission for cluster and galaxies.

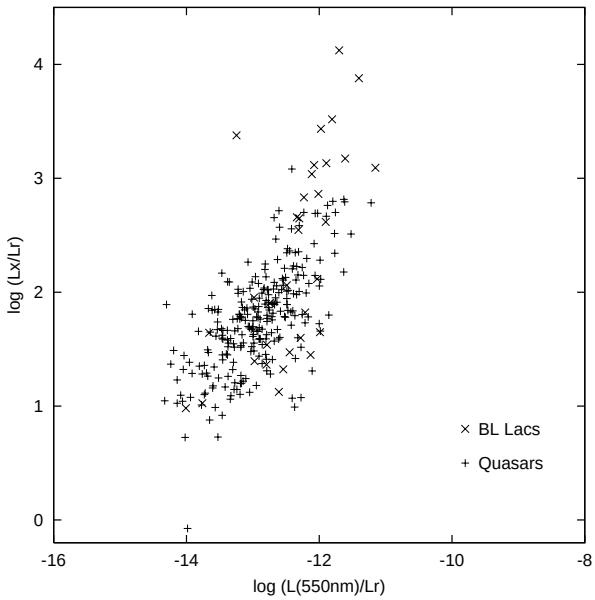

Fig. 21. The luminosity ratios as in Fig. 20, but for BL Lacs and quasars.

7. Luminosities

For sources with measured redshifts we have calculated the K-corrected luminosities assuming a Friedman cosmology with $H_0 = 50\,\mathrm{km\ s^{-1}\ Mpc^{-1}}$, $q_0 = 0.5$ and isotropic emission. We show the resulting distributions in Fig. 18 and Fig. 19 for radio and X–ray luminosities, respectively. Mostly galaxies are seen at lower luminosities. The properties of optically identified sources in our sample are very similar to those discussed in B95 (their Fig. 10a and Fig. 10b). The distance independant luminosity ratios shown in Fig. 20 and Fig. 21 for different classes of sources corresponding to Fig. 10c of B95 are very similar too, although the present sample omits the weaker radio sources compared to the B95 sample. A discussion of the luminosities, their correlation and implications was already given by B95 and our sample does not alter any conclusion derived in this investigation.

We do not find any dependence of the percentage polarization on the X–ray or radio luminosity. This is not unexpected and in accordance with the missing dependence of the percentage polarization on redshift as it was already shown in Sect. 5.

8. Conclusion

We have presented the radio properties of a large sample of 741 radio-loud X–ray sources from the ROSAT Survey, which are in their vast majority AGN. This sub-sample of radio identifcations consists of sources stronger than about 100 mJy at

6 cm wavelength and has a higher fraction of identifications, when compared to the entire source sample. The X–ray source sample is somewhat biased by sensitivity and spectral variations across the sky due to the increasing HI–column density towards the Galactic plane. With increasing z the average X–ray flux density decreases as expected. The radio sample shows increasing redshift with increasing flux density. In addition the sample shows a larger fraction of compact sources and more flat spectrum sources than an unbiased radio sample. We also find a slight excess of polarized sources ($> 3\%$) if compared to other radio source samples.

Compared to previous similar studies where radio flux densities of AGN are compared with their X–ray emission an interesting new aspect are the large RMs observed for the ROSAT selected radio sources. As shown in Fig. 10 there is a clear excess of RM if compared to a large unbiased source sample, which certainly contains some fraction of X–ray loud sources. Therefore the derived average excess of about 45 $\mathrm{rad\ m^{-2}}$ has to be considered as a lower limit.

Extragalactic sources visible in the soft X–ray range require low internal absorption. Preferably sources looked at face on or with large inclination angles are visible following current unification schemes (e.g. Urry & Padovani 1995). The increase of the average redshift with radio flux density and the flatter radio spectra support this view as these radio characteristics indicate a large fraction of beamed radio emission. The X–ray emission itself seems not to be beamed significantly. This holds also for the γ-ray emitting EGRET sources, where strong beaming is expected in the γ-ray and the radio range, but where the lowest ratios of the X–ray to radio flux densities are noted (Fig. 14). An exception are the TeV–sources MKN 421 and MKN 501, where the X–ray emission seems to be beamed as well and as a result exceeds the average ratio of the X–ray to radio emission significantly. Excessive RMs are noted, which however, seem mainly connected to steep spectrum and to extended sources and thus are unlikely due to a beamed component. This result is certainly not in contradiction to the suggested large inclination angles.

Another difference of the present study to previous investigations is the quasi-simultaneously observed radio spectrum for the majority of sources. This is in particular important for sources with an inverted spectrum (Table 7), which are mostly variable and therefore do not allow to combine data from different epochs. For sources with flat or steep spectra the differences to the data from the literature are generally small.

We conclude that the properties of X–ray selected radio sources are in agreement with current unification schemes in that X–ray loud AGN are preferably seen face-on. This orientation increases the fraction of beamed radio emission to the total flux density compared to source samples with a more random distribution of viewing angles.

Acknowledgements. We like to thank the operators at the Effelsberg 100-m telescope for their support during the long observing runs. The ROSAT project is supported by the Bundesministerium für Bildung, Wissenschaft, Forschung und Technologie and the Max-Planck-Gesellschaft. We thank our colleagues from the ROSAT group for their support. This research has made use of the NASA/IPAC Extragalactic Data Base (NED) which is operated by the Jet Propulsion Laboratory, California Institute of Technology, under contract with the National Aeronautics and Space Administration.

References

Atkins R., Benbow W., Berley D., et al., 1999, ApJ 525, L25
Boller Th., Bertoldi F., Dennefeld M., Voges W., 1998, A&AS 129, 87
Brinkmann W., Siebert J., Boller Th., 1994, A&A 281, 355
Brinkmann W., Siebert J., Reich W., et al., 1995, A&AS 109, 147 (B95)
Brinkmann W., Yuan W., Siebert J., 1997a, A&A 319, 413
Brinkmann W., Siebert J., Feigelson E.D., et al., 1997b, A&A 323, 739 (B97)
Condon J.J., Broderick J.J., Seielstad G.A., 1989, AJ 97, 1064
Dickey J.M., Lockman F.J., 1990, ARA&A 28, 215
Kühr H., Nauber U., Pauliny-Toth I.I.K., Witzel A., 1979, MPIfR preprint No. 55
Kühr H., Pauliny-Toth I.I.K., Witzel A., Nauber U., 1981, A&AS 45, 367
Laurent-Muehleisen S.A., Kollgaard R.I., Ryan P.J., et al., 1997, A&AS 122, 235 (L97)
Loiseau N., Reich W., Wielebinski R., Reich P., Münch W., 1988, A&AS 75, 67
McMahon R.G., 1991, In: Crampton D. (ed.) The Space Distribution of Quasars. ASP Conf. Series Vol. 21, p. 129
Neumann M., Reich W., Fürst E., et al., 1994, A&AS 106, 303 (N94)
Okudaira A., Tabara H., Kato T., Inoue M., 1993, PASJ 45, 153
Ott M., Quirrenbach A., Krichbaum T.P., et al., 1994, A&A 284, 331
Punch M., Akerlof C.W., Cawley M.F., et al., 1992, Nat 358, 477
Quinn J., Akerlof C.W., Biller S., et al., 1996, ApJ 456, L83
Reich W., Steppe H., Schlickeiser R., et al., 1993, A&A 273, 65
Reich W., Reich P., Pohl M., Kothes R., Schlickeiser R., 1998, A&AS 131, 11
Schartel N., 1995, Ph.D. Thesis, University of München
Siebert J., Brinkmann W., Drinkwater M.J., et al. 1998, MNRAS 301, 261
Simard-Normandin M., Kronberg P.P., Button S., 1981, ApJS 45, 97 (SKB)
Simard-Normandin M., Kronberg P.P., Button S., 1982, A&AS 48, 137,
Stark A.A., Gammie C.F., Wilson R.W., 1992, ApJS 79, 77
Tabara H., Inoue M., 1980, A&AS 39, 379
Trümper J., 1983, Adv. Space Res. Vol. 2, No. 4, 241
Urry C.M., Padovani P., 1995, PASJ 107, 803
Voges W., 1992, In: Proc. of the ISY Conference: Space Science. ESA ISY-3, ESA Publications, p. 9
Voges W., Aschenbach B., Boller Th., et al., 1999, A&A 349, 389
Welter G.L., Perry J.J., Kronberg P.P., 1994, ApJ 279, 19
Zukowski E.L.H., Kronberg P.P., Forkert T., Wielebinski R., 1999, A&AS 135, 571